Statistical Study of the Corrosion Behavior of Al_2CuMg Intermetallics in AA2024-T351 by SKPFM

Loïc Lacroix,[a] Laurence Ressier,[b] Christine Blanc,[a,*,z] and Georges Mankowski[a]

[a]*Centre Interuniversitaire de Recherche et d'Ingénierie des Matériaux, UMR CNRS 5085, Ecole Nationale Supérieure des Ingénieurs en Arts Chimiques et Technologiques, 31077 Toulouse Cendex 04, France*
[b]*Laboratoire de Physique et Chimie des Nano-Objets, UMR CNRS 5215, Institut National des Sciences Appliquées, 31077 Toulouse Cedex 04, France*

A statistical study combining atomic force microscopy, scanning Kelvin probe force microscopy (SKPFM), and energy-dispersive spectroscopy was carried out on more than 300 Al_2CuMg intermetallic particles of AA2024 alloy to determine their corrosion behavior in chloride-containing solutions. The combination of these three techniques allowed the correlation of the dissolution depth of the S-phase particles to their SKPFM potential and their chemical composition. This study also revealed that SKPFM measurements must be carried out with many precautions, but it is a powerful tool for the study of localized corrosion.
[DOI: 10.1149/1.2799089]

Aluminum alloys such as the 2XXX series are widely used in the aircraft industry due to their high strength-to-weight ratio. But, these alloys are extremely susceptible to localized corrosion in chloride-containing media and different kinds of corrosion are observed such as pitting corrosion,[1,2] intergranular corrosion (IGC),[3,4] exfoliation,[5] and stress corrosion cracking.[6,7]

Corrosion susceptibility of 2XXX series Al alloys has long been studied.[3,8-12] It is mainly caused by their heterogeneous microstructure, which is intentionally introduced in order to improve the mechanical properties. Among the different types of intermetallic particles present in AA2024 alloy, Al_2CuMg particles (called S-phase) are widely studied because they are very reactive and are present both in the grain boundary and in the grains and they constitute a large proportion of the particles present in 2XXX alloys.[13,14] Corrosion damage is localized at the S-phase particles, resulting in selective dissolution or pitting in the matrix adjacent to the particle.[15-19] This phenomenon has often been studied by electrochemical measurements in combination with scanning electron microscopy (SEM) and energy-dispersive spectroscopy (EDS). However, common electrochemical methods lack micrometer-scale lateral resolution, which is critical for understanding the role of intermetallic particles in localized corrosion.

For about 10 years, the combination of topographical analysis by atomic force microscopy (AFM) in air or in solution (in situ) with potential mapping in air by scanning Kelvin probe force microscopy (SKPFM) has appeared to be a powerful tool to study the localized corrosion of AA2024 alloy.[20-24] In fact, the potential measured by SKPFM shows a clear chemical contrast allowing various metallurgical phases or materials down to 100 nm in size to be differentiated with potential noise smaller than 1 mV.[24,25] Even though measurements are performed in air, Schmutz et al. have shown that the SKPFM potential gives a good measure of the practical nobility of intermetallics in AA2024 because this potential and the corrosion potential measured in solution seem to be correlated.[20] But, SKPFM measurements and analyzes have to be performed with many precautions because the relationship between SKPFM potentials and local electrochemistry is relevant but not trivial.[26] In fact, SKPFM measurements are highly influenced by the structure, composition, and thickness of the oxide film covering the surface, surface charge distribution, and adsorbed species at the surface.[22,24] As recently mentioned by Rohwerder et al., the correlation between the SKPFM potential and the corrosion potential is not of general validity, which makes systematic studies necessary.[27] Furthermore, previous AFM/SKPFM studies on AA2024 reported in the literature have always been performed on a small number of intermetallics, making any quantitative extrapolation on the macroscopic corrosion behavior of this alloy quite difficult. Therefore, statistical studies on the extent of correlation between corrosion behavior and SKPFM potentials are important.

In this study, AFM and SKPFM measurements were performed on more than 300 S-phase particles of the 2024 T351 alloy before and after immersion in chloride-containing sulfate solutions to study their dissolution mechanism using a statistical approach. These analyzes by scanning probe microscopy were then related to the chemical composition of the S-phase particles as determined by EDS.

Experimental

Material.— An AA2024 T351 rolled plate (wt %: Cu 4.50, Mg 1.44, Mn 0.60, Si 0.06, Fe 0.13, Zn 0.02, and Ti 0.03) with a thickness of 50 mm was used for this study. The T351 temper corresponds to a solution heat-treatment at 495°C (± 5°C), water quenching, straining, then tempering at room temperature for 4 days.

Microstructure and chemical composition of the S-phase particles.— Samples were observed before and after immersion in chloride-containing sulfate solutions by SEM using a Leo 435VP apparatus. The compositional analysis of the intermetallic particles was determined with EDS by averaging the results obtained over a large number of particles. An accelerating voltage of 15 kV was used for both secondary electron imaging and EDS analyses.

AFM and SKPFM measurements.— AFM and SKPFM measurements were performed on a Nanoscope IIIa multimode atomic force microscope from Digital Instruments equipped with a Basic Extender electronic module.

The probes selected were conductive Pt/Ir-coated silicon tips (resistivity 0.01–0.025 Ω cm) on a cantilever whose resonant frequency was 75 kHz. These long and slender tips with an apex radius of about 25 nm on a cantilever of small width and surface area have optimum geometric characteristics to obtain a good resolution in potential maps.[28]

To minimize cross-talk, topography and potential scans were collected using the "lift" technique, which involves a two-pass rastering of the surface. On the first pass, the surface topography of a single line scan is acquired by standard tapping mode. On the second pass, at a set lift height from the sample surface, the drive piezo that normally vibrates the cantilever in tapping mode is turned off and an oscillating voltage V_{AC} sin ωt (with $\omega/2\pi$ near the resonant frequency of the cantilever) is directly applied to the cantilever tip to measure the surface potential. Any dc voltage difference between the tip and the sample generates an oscillating electric force on the cantilever which causes the cantilever to vibrate. The local SKPFM potential is thus determined by adjusting the dc voltage on the tip until the oscillation amplitude of the cantilever becomes zero. At

* Electrochemical Society Active Member.
z E-mail: Christine.Blanc@ensiacet.fr

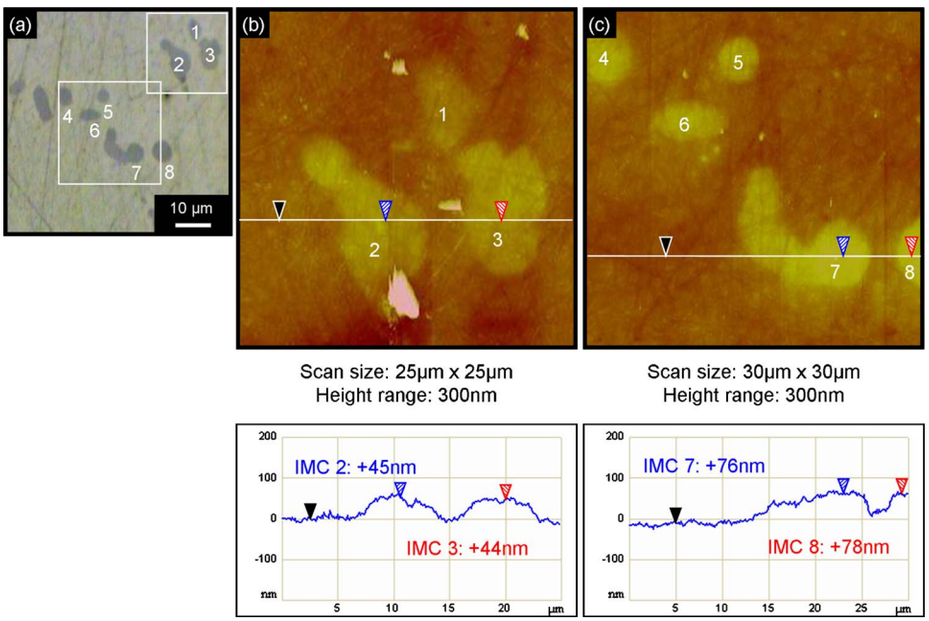

Figure 1. (Color online) Observations of an as-polished AA2024 sample: (a) optical micrograph with eight S-phase intermetallic particles, (b) AFM top view of particles 1–3 as in (a) and sections of intermetallics (IMCs) 2 and 3, (c) AFM top view of intermetallics 4–8 as in (a) and sections of particles 7 and 8. In the sections, both measurements were made with reference to the black cursor.

this point the tip voltage is the same as the local surface potential. Images are obtained by repeating this procedure for each line along the slow-scan axis. The voltage applied to the cantilever tip is recorded to construct a potential map of the sample with respect to the tip used.

In this study, all AFM and SKPFM measurements were made in air at room temperature and an ambient relative humidity of about 40%. Potential mapping by SKPFM was carried out at a lift height of 50 nm, which was found to be the optimal value to limit cross-talk with topography and obtain a lateral resolution better than 100 nm with a good signal-to-noise ratio of the potential data. A drive amplitude V_{AC} of 6 V was chosen to make sensitive potential measurements, taking into account parametric amplification.[29] The feedback electronics was finely tuned to give the highest sensitivity.[30] A scan rate of 0.5 Hz was used for all the measurements on samples before immersion. On highly corroded S-phase particles, scan rates as low as 0.1 Hz were sometimes required to accurately map the topography, which is a crucial prerequisite to get nonerroneous SKPFM potential mapping.[24]

Contrary to some authors who invert the SKPFM potential data in order to obtain the same polarity as the electrochemical potentials,[20] here all the potential maps presented used raw data. Because we often checked that the tip used was stable in potential and we were only interested in potential differences between the S-phase particles and the matrix, we did not need to calibrate the potential measurements by comparison to the potential measured on pure Ni or Pt.[20,21,24] By assuming that, far from the particles, there is no significant variation of the matrix potential, we defined the potential of an S-phase particle by the difference of the SKPFM potential between the S-phase particle and the matrix remote from the particle. The potential of S-phase particles is thus denoted in the following as "SKPFM potential." Measurements performed on a Ag–Al couple showed that the difference of SKPFM potential between Ag and Al was negative, so a potential lower for an intermetallic than that of the matrix means that the intermetallic is nobler than the matrix.

The samples used for AFM and SKPFM measurements were $4 \times 2 \times 2$ mm parallelepipeds embedded in epoxy resin with an 8 mm^2 area exposed to the electrolyte. Special care was taken for sample preparation, which is crucial for obtaining reliable results.[31] The samples were mechanically polished with up to 4000 grit SiC paper, then with 3 µm diamond paste, down to 1/4 µm diamond paste using ethanol as lubricant. The samples were finally ultrasonically cleaned in ethanol and dried in air. Ethanol was chosen as lubricant instead of water or petroleum ether because it was found to lead to a smooth surface (mean roughness $R_a = 4.7 \pm 0.5$ nm on 1000 μm^2 areas) with no dissolution of S-phase particles during polishing.

Corrosion tests consisted of immersion at the open-circuit potential in a 0.1 M Na_2SO_4 solution with 0.001 M NaCl at room temperature. All chemicals used were analytical reagent grade and water was deionized. For each sample, AFM and SKPFM measurements were performed before and after immersion in several areas (where the only particles present were S-phase particles), leading to a statistical analysis on more than 300 particles. The sample surface was always prepared just before AFM and SKPFM measurements. Special care was taken for corroded samples; before any drying, the samples were ultrasonically cleaned in water to dissolve the corrosion products and to avoid any precipitation of sulfate and chloride crystals from drying solution. The samples were finally ultrasonically cleaned in ethanol and air dried to limit any effect of the adsorbed layer on the potentials.

Results and Discussion

Study of S-phase particle dissolution by combining AFM, SEM, and optical microscopy.— Figure 1 shows typical observations of an as-polished AA2024 sample. In the optical micrograph (Fig. 1a), eight Al_2CuMg particles (numbered from 1 to 8) can be distinguished due to their round shape compared to the irregular shape of the Al–Cu–Mn–Fe particles. In agreement with previous studies, the AFM observations (Fig. 1b and c) reveal that these Al_2CuMg particles protrude slightly from the surface because of their greater hardness and lower rate of polishing relative to the matrix.[20] AFM measurements on about 300 S-phase particles of six different samples revealed that their mean height relative to the matrix was 60 ± 26 nm and their mean area 46 ± 38 μm^2.

Figure 2 presents typical observations of the same sample area after an immersion of 60 min in a 0.1 M Na_2SO_4 + 0.001 M NaCl solution. Comparison of Fig. 1 and 2 clearly reveals that there is a great dispersion in the kinetics of corrosion initiation or/and propagation from one Al_2CuMg particle to another; intermetallics 1, 2, 3, 7, and 8 are corroded, while particles 4, 5, and 6 appear uncorroded. Furthermore, among the corroded particles, some (particles 2 and 7) are partially dissolved over their whole surface. This dissolution can be explained by the aluminum and magnesium dealloying as often

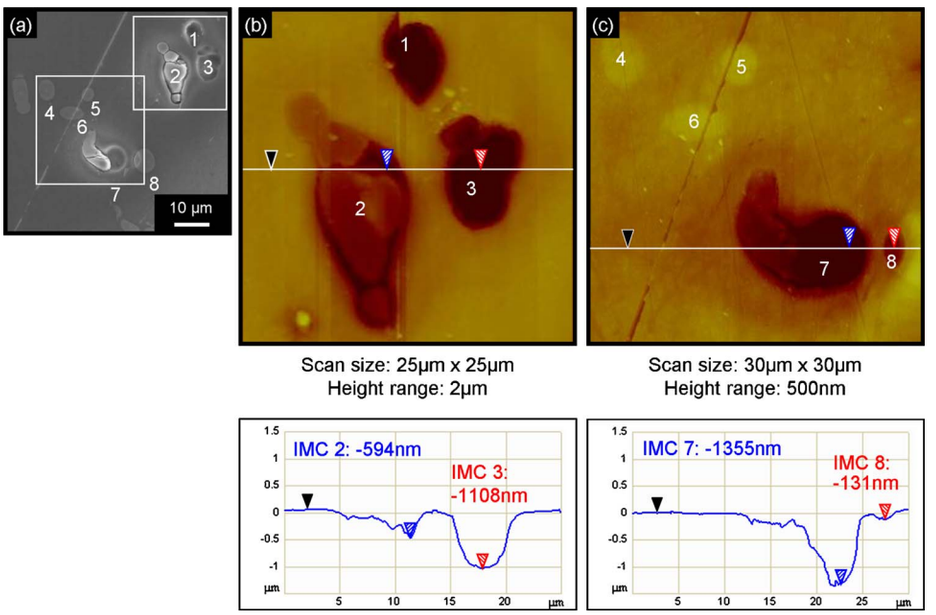

Figure 2. (Color online) Observations of the same AA2024 area as in Fig. 1 after immersion in a 0.1 M Na_2SO_4 + 0.001 M NaCl solution for 60 min at the open-circuit potential: (a) SEM micrograph, (b) AFM top view of S-phase particles 1–3 as in (a) and sections of intermetallics (IMCs) 2 and 3, (c) AFM top view of particles 4–8 as in (a) and sections of intermetallics 7 and 8. In the sections, both measurements were made with reference to the black cursor.

referenced in the literature.[14] It can also be observed that a groove was formed around the whole perimeter of the particle as seen on both the SEM micrograph (Fig. 2a) and the topographical AFM map (Fig. 2b and c). Assuming that there was no dissolution of the matrix beyond some micrometers, the dissolution of the S-phase particles reached 639 nm (594 + 45 nm) and 1431 nm (1355 + 76 nm) for particles 2 and 7, respectively. Due to the great dispersion in the kinetics of corrosion initiation or/and propagation, other particles (particles 1 and 3) are more corroded; they are completely dissolved or maybe removed due to the growth of the groove around the perimeter of the particles. These observations confirm previous studies;[11,17] when AA2024 alloy is immersed in chloride-containing solutions, dissolution of both S-phase particles and the surrounding matrix is observed.

In summary, these observations reveal a small dispersion of the S-phase particle height on as-polished samples but a great heterogeneity in the reactivity of the S-phase particles. A statistical analysis is thus absolutely necessary for any accurate study of the dissolution of the S-phase particles and to explain the macroscopic corrosion behavior of 2024 aluminum alloy.

About 150 S-phase particles on three AA2024 samples were thus analyzed by AFM in tapping mode before and after immersion for 2 h (samples A, B, and C) in a 0.1 M Na_2SO_4 + 0.001 M NaCl solution. The mean dissolution depth of each particle (calculated as the ratio of its dissolved volume to its area before immersion) was plotted vs its area (exposed to the electrolyte during immersion) in Fig. 3 for the three different samples. This graph exhibits: (*i*) a huge dispersion of the S-phase particle reactivity on any single sample: the mean dissolution depth of an S-phase particle exposed to the same corrosive conditions varies from 30 to 530 nm [mean 200 ± 130 nm standard deviation (SD)], from 40 to 460 nm (mean 200 ± 120 nm SD), and from 233 to 614 nm (mean 436 ± 157 nm SD) for samples A, B, and C, respectively. This heterogeneity of the corrosion behavior from one S-phase particle to another could be related to differences in the chemical composition of the oxide film at its surface (protecting it from dissolution for a given time) or to defects in the oxide film; (*ii*) a reproducible dispersion of the S-phase particle reactivity from one sample to another (SD of the mean dissolution depth: 130, 120, and 157 nm for samples A, B, and C, respectively); and (*iii*) no influence of the particle area exposed to the electrolyte on its reactivity.

Furthermore, Fig. 2 shows the great dispersion of reactivity from one particle to another on the same sample, but it also proves that the dissolution of an S-phase particle can be heterogeneous. Figures 2a and c show, for example, that only a small part of particle 8 is dissolved while the other part remains uncorroded. Besides, the dissolution depth of particles 2 and 7 varies from one point on the particle to another. Thus, the description of S-phase particle dissolution has to be considered carefully. In Fig. 3, the mean dissolution depth of each S-phase particle was calculated as the ratio of its dissolved volume to its area. A finer approach consisting of a local study of the dissolution phenomenon was necessary to accurately relate the dissolution of the S-phase particles to SKPFM and EDS measurements. The local dissolution depth was then measured at a particular point on a particle and can be related to its local chemical composition and its local SKPFM potential at the same point.

Correlation between AFM, SKPFM, and EDS measurements.— Figure 4 shows an AFM topographical map (Fig. 4a) and the corresponding SKPFM potential map (Fig. 4b) of an as-polished AA2024 sample. Four Al_2CuMg particles (numbered from 1′ to 4′) were marked in particular. Comparison of Fig. 4a and b reveals that the high contrast on the SKPFM potential map between the S-phase particles and the aluminum matrix allows the intermetallics to be clearly located and identified, in agreement with previous studies.[20,22] Sections of the potential maps revealed a difference of

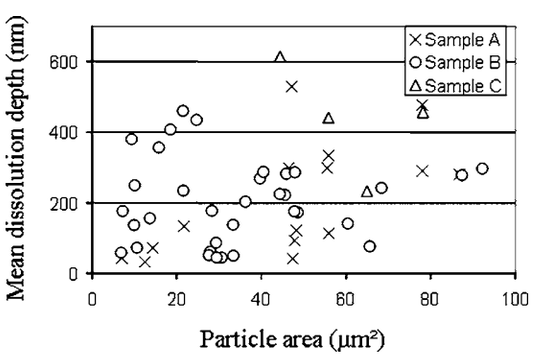

Figure 3. Mean dissolution depth vs particle area (exposed to the electrolyte during immersion) for Al_2CuMg intermetallics on an AA2024 alloy immersed for 2 h in a 0.1 M Na_2SO_4 + 0.001 M NaCl solution at open-circuit potential. Three samples, referred to as A, B, and C, were analyzed.

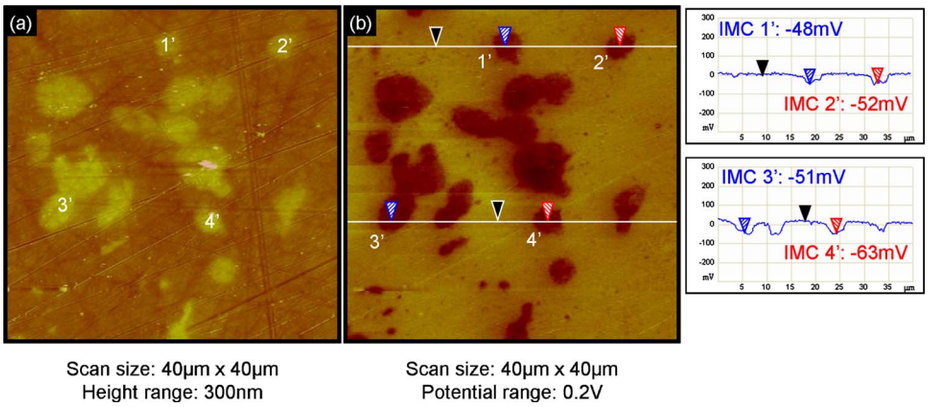

Figure 4. (Color online) Observations of four S-phase intermetallics (IMCs 1′–4′) on an as-polished AA2024 sample: (a) AFM and (b) SKPFM potential maps with two associated sections. In the sections, both measurements were made with reference to the black cursor.

potentials with respect to the matrix of −52 and −51 mV for particles 2′ and 3′, respectively. In agreement with previous studies, S-phase particles appear less active than the matrix (the displayed potential data are raw data, not inverted).[20,22,23] The same measurements were performed on the same sample in the same zone after immersion in a 0.1 M Na_2SO_4 + 0.001 M NaCl solution at open-circuit potential for 1 h (Fig. 5). Both SEM and AFM observations (Fig. 5a and b) show that particle 1′ is not corroded while particles 2′ and 3′ are highly dissolved (dissolution of the surrounding matrix is also observed). Particle 4′ was removed from the surface certainly due to the strong dissolution of the surrounding matrix. The corresponding SKPFM potential map (Fig. 5c) shows that for particles 2′ and 3′, the contrast is stronger than before immersion; particles 2′ and 3′ present a difference of SKPFM potential with respect to the matrix of about −143 and −293 mV, respectively. This shows that the dissolution of S-phase particles leads to an increase (in absolute value) of the difference in potential with respect to the matrix. For particle 4′, which is completely dissolved, there is no longer a potential difference with respect to the matrix, which is easily understandable because, the particle having being removed, the potential measured is that of the matrix. Figure 5c also shows that for particle 1′, there is no contrast in SKPFM potential after immersion even though the particle is still present and intact, probably due to the formation of a thick oxide layer over the top.

Statistical analysis of the SKPFM potential of S-phase particles confirms and quantifies the tendencies observed in Fig. 5. As said previously, we defined the potential of an S-phase particle by the difference of the SKPFM potential between the S-phase particle and the matrix remote from the particle. Figure 6a shows the distribution of this potential measured for about 300 S-phase particles on an as-polished AA2024 alloy. A similar distribution was plotted for the corroded particles after immersion for 60 min in a 0.1 M Na_2SO_4 + 0.001 M NaCl solution (Fig. 6b).

Figure 6a shows that the SKPFM potential values for the particles before immersion were significantly scattered with values varying from −20 to −240 mV (mean value −90 mV with a SD of 45 mV). Taking account of the fact that these values are raw noninverted data for all the particles present, they are in quite good agreement with values reported in the literature for just one or only a few particles (+280,[20] +200,[23] and +150 mV[24]).

After immersion in the aggressive solution, the SKPFM potentials measured with respect to the matrix are more scattered; they

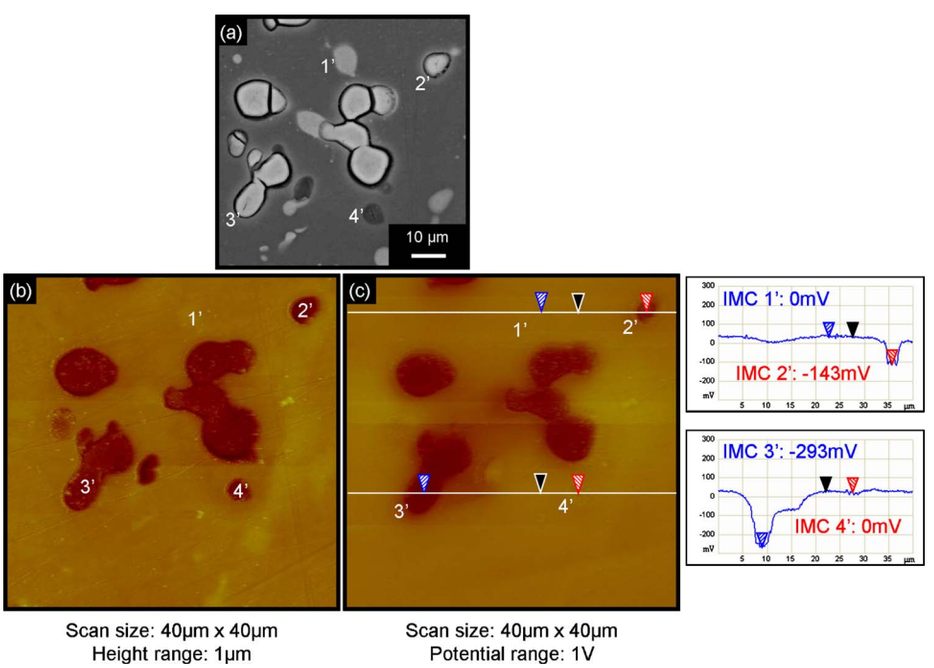

Figure 5. (Color online) Observations of the same area as in Fig. 4 (IMCs 1′–4′) after immersion for 60 min in a 0.1 M Na_2SO_4 + 0.001 M NaCl solution at open-circuit potential: (a) SEM observation and (b) AFM and (c) SKPFM potential maps with two associated sections. In the sections, both measurements were made with reference to the black cursor.

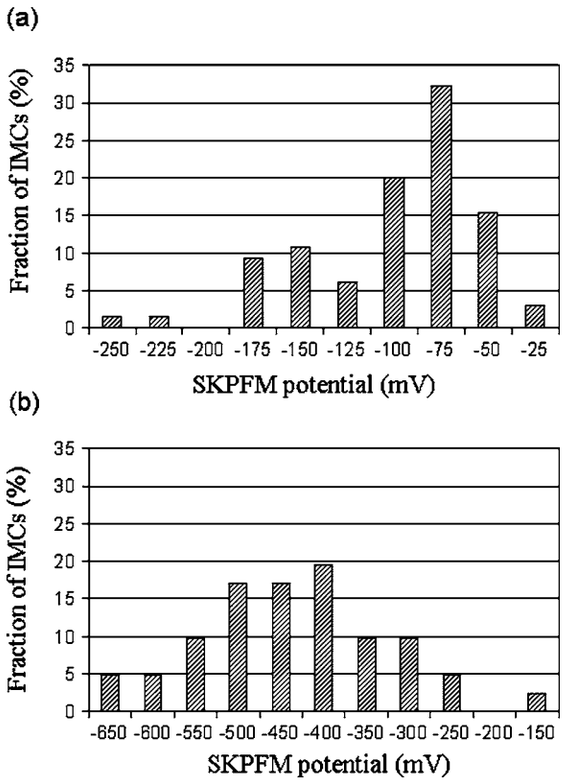

Figure 6. Distribution of the SKPFM potential of S-phase particles relative to the matrix (a) on an as-polished AA2024 sample and (b) after immersion for 60 min in a 0.1 M Na_2SO_4 + 0.001 M NaCl solution.

decrease down to a value varying from −130 to −650 mV (mean −410 ± 110 mV SD) (Fig. 6b). This increase (in absolute value) of the potential difference has already been reported in the literature but has only been quantified on a few particles.[23]

It can be assumed that the SKPFM potential is related to the chemical composition of the first monolayers of the sample.[22] When the particles are dissolved, the increase of the contrast in potential strongly suggests that the chemical composition of the particles also changes. Local EDS analysis was thus performed on all particles for which potential measurements were carried out. The results reveal that all the S-phase particles (EDS analysis performed on 20 particles using standard samples for calibration) have the same chemical composition before immersion: 52.6 ± 0.5 atom % Al, 22.1 ± 0.2 atom % Cu, 25.1 ± 0.3 atom % Mg. This shows that the scattering on the SKPFM potentials for the as-polished sample cannot be attributed to variations in the chemical composition of the intermetallics detectable with EDS. However, EDS analysis is not a surface-sensitive technique and cannot be used to detect low variations of the chemical composition of the extreme surface of the intermetallics. Furthermore, other parameters, some of them being invisible to standard surface analysis, have to be considered, such as the chemical composition, the thickness and defect structure of the oxide film covering the particle, the environmental parameters during the formation and age of the oxide film, the surface preparation, and maybe the crystallographic orientation of the particles.[23-25,28,30-32] Comparison of Fig. 4 and 5 previously showed that the SKPFM potential of an uncorroded particle becomes quite similar to that of the matrix after a long immersion time due to thickening of the oxide film during immersion in the electrolyte. This result is in perfect agreement with observations made by Schmutz et al.,[21] Leblanc et al.,[23] and Muster et al.[24] Because the SKPFM potential characterizes a thin layer at the surface of the material, there is no significant influence on the potential measure-

)

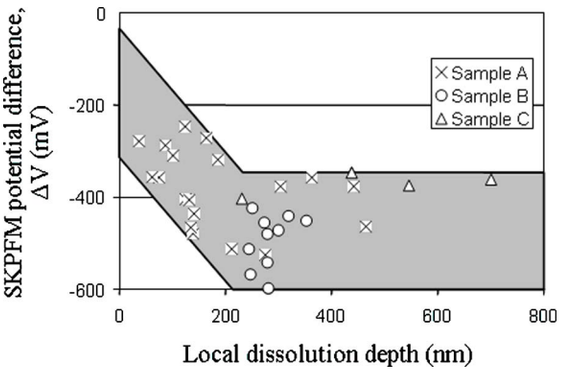

Figure 7. Variation of the local SKPFM potential of the S-phase particles relative to the matrix with immersion $\Delta V = (V_{particle} - V_{matrix})_t - (V'_{particle} - V'_{matrix})_0$ vs the local dissolution depth after immersion in a 0.1 M Na_2SO_4 + 0.001 M NaCl solution (samples A–C).

ments of the material under the oxide film. Furthermore, the oxide layers formed on the matrix and on Al_2CuMg particles obviously differ in their chemical composition[16,33] but the SKPFM potential measurements are not sensitive enough to reveal such differences with high contrast.

In brief, the dispersion of the SKPFM potentials for the S-phase particles before immersion could be related to different parameters, such as some differences in the thickness of the oxide films (not to some differences in the chemical composition) formed on the S-phase particles corroborating the high dispersion in reactivity. The increased scattering of the SKPFM potentials for the corroded S-phase particles could be related to their differences in reactivity, leading to different alterations of the chemical composition of the particles after immersion.

Because of the great dispersion of SKPFM potential data before and after immersion from one particle to another, it is necessary to consider, for each particle, the difference between its potential after immersion V_t and that on the as-polished sample V_0 to accurately represent the phenomenon. Figure 7 reveals that a good correlation exists between the variation $\Delta V = (V_{particle} - V_{matrix})_t - (V'_{particle} - V'_{matrix})_0$ of the local SKPFM potential of the S-phase particles relative to the matrix with immersion and their local dissolution depth at the same point. When a particle is dissolved, its potential becomes more and more different from that of the matrix until it reaches a critical value for a dissolution depth of about 250 nm. Figure 8 shows the local chemical composition of the S-phase particles (expressed as Cu, Al, and Mg contents) vs their local dissolution depth. These graphs show that the dissolution of an S-phase particle parallels a significant decrease of its magnesium content from 25 to nearly 0 atom % and a strong copper enrichment from 25 to 70 atom %. These results are in good agreement with literature because it has often been shown that copper enrichment occurs during the dissolution of S-phase particles.[13,14,17,18,23] The copper enrichment of the particles is well correlated with the increase of the potential difference between the S-phase particles and the matrix $\Delta V = (V_{particle} - V_{matrix})_t - (V'_{particle} - V'_{matrix})_0$. Due to an alteration of its chemical composition with copper enrichment, the S-phase particle becomes nobler during immersion, explaining partially the dissolution of the surrounding matrix with the formation of a groove around the perimeter of the particles. This mechanism can be followed by the measurement of the variation of the SKPFM potential of the particle after immersion.

As previously demonstrated, there is a great dispersion both in the reactivity of the S-phase particles (some are not corroded while others strongly dissolve) and in the SKPFM potentials of the S-phase particles before immersion. One could wonder if SKPFM could be used as a predictive tool for the corrosion behavior of the

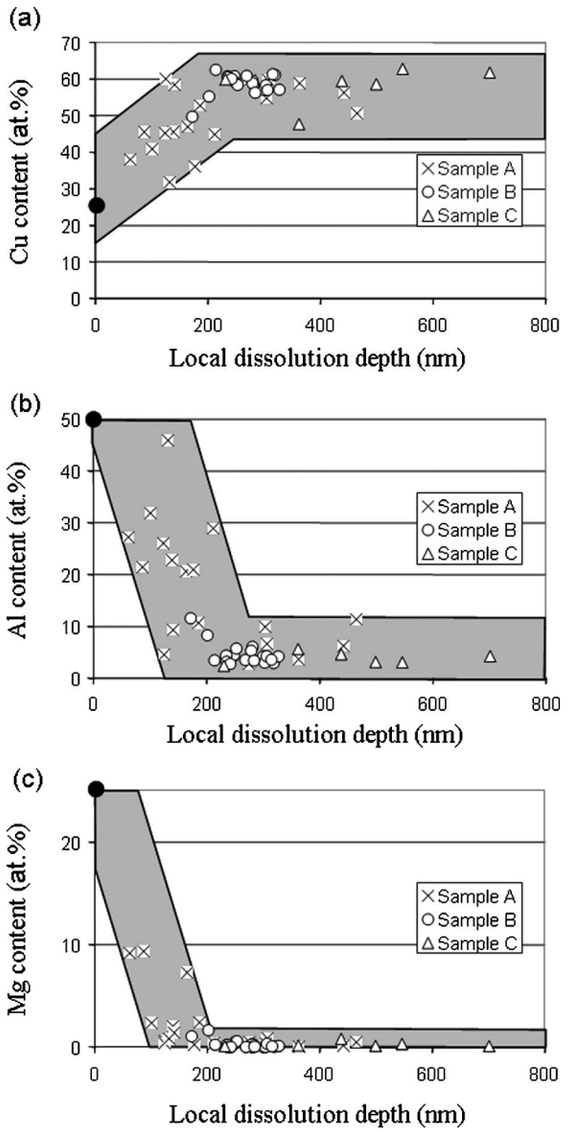

Figure 8. Local chemical composition of the S-phase particles expressed as (a) Cu content, (b) Al content, and (c) Mg content vs their local dissolution depth after immersion in a 0.1 M Na_2SO_4 + 0.001 M NaCl solution (samples A–C). The black points indicate the element (Cu, Al, or Mg) content of the intermetallics on the as-polished sample.

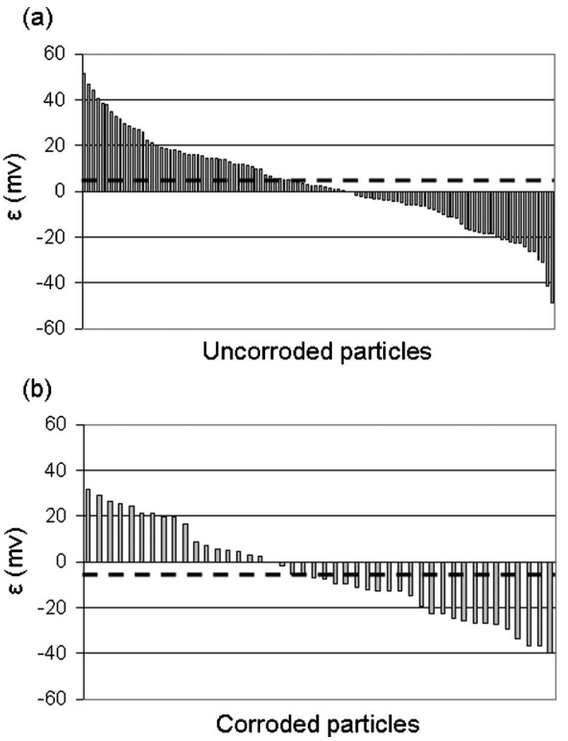

Figure 9. Deviation ε of the SKPFM potential measured for each particle before immersion from the mean value of the SKPFM potential before immersion obtained with the SKPFM potentials of all the particles. The parameter ε is defined as $\varepsilon = (V_{particle} - V_{matrix})_0 - \Sigma_n(V_{particle} - V_{matrix})_0/n$, where n is the total number of particles: (a) particles found uncorroded and (b) particles corroded after immersion in a 0.1 M Na_2SO_4 + 0.001 M NaCl solution at open-circuit potential. The dashed lines indicate the mean value of ε for (a) uncorroded and (b) corroded particles.

S-phase particles. It would be interesting to check this assumption. Therefore, a statistical analysis of the potentials measured for 300 S-particles before immersion was performed. A correlation between the potential values and the corrosion behavior of the intermetallics was made. Figure 9 shows the deviation, noted as ε, of the SKPFM potential measured for each particle before immersion from the mean value of the SKPFM potential before immersion obtained with the potentials of all the particles. The parameter ε was thus defined as $\varepsilon = (V_{particle} - V_{matrix})_0 - \Sigma_n(V_{particle} - V_{matrix})_0/n$, where n is the total number of particles. Two cases were taken into account: particles which were found to be uncorroded after immersion in the electrolyte (Fig. 9a) and those which were corroded after immersion (Fig. 9b). The mean value of ε was calculated for both uncorroded particles and corroded particles; these two values are represented by the dashed lines on the graph. The mean value of ε for the uncorroded particles is positive (and equal to 4 mV), while that for the corroded particles is negative (and equal to −5 mV). Therefore, it could be concluded that the lower the SKPFM potential of an intermetallic before immersion, the stronger its reactivity during immersion. However, it is necessary to point out that the difference between the two mean ε values (for uncorroded and for corroded particles) is not significant in comparison to potential resolution. Thus, it seems difficult to give a clear answer about the predictive aspect of SKPFM measurements which is in good agreement with the precautions recommended by Rohwerder et al. when conclusions are given from SKPFM measurements performed on as-polished samples.[27]

Figures 10 and 11 show, as previously mentioned in Fig. 2, that the dissolution kinetics of an S-phase particle can vary significantly inside the particle. Figures 10a and b correspond to SEM observations of an AA2024 sample before and after a 30 min immersion in chloride-containing sulfate solutions. Figure 10b shows two areas surrounded by a dotted line which appear darker than the other parts of the particles. These two areas were dissolved while no corrosion was observed elsewhere. Particular attention was paid to two parts of the same Al_2CuMg particle with different reactivities. The first part, α, was not corroded, while the other, β, dissolved. Figure 11 shows the EDS analyses performed on these two parts before (α_0 and β_0) and after immersion (α_t and β_t); for α (Fig. 11a) no variation of the chemical composition is observed, while for β (Fig. 11b) a strong copper enrichment with magnesium dissolution can be noticed. For quantitative EDS analysis, calibration was performed using standard samples. The results also show the presence of oxygen; the composition of the oxide covering the corroded particle is about 30 atom % oxygen and 60 atom % copper. Of course, this analysis is not very accurate due to the size of the interaction area between

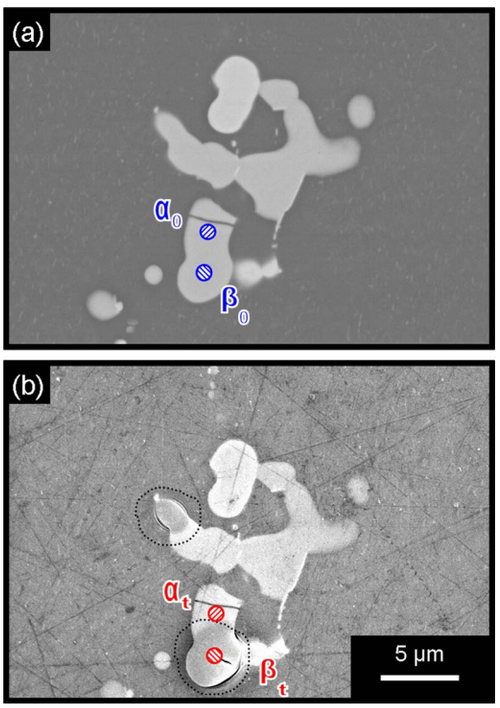

Figure 10. (Color online) SEM observations of an AA2024 sample (a) before and (b) after immersion for 30 min in a 0.1 M Na_2SO_4 + 0.001 M NaCl solution at open-circuit potential. Two zones, α and β, are indicated on an S-phase particle.

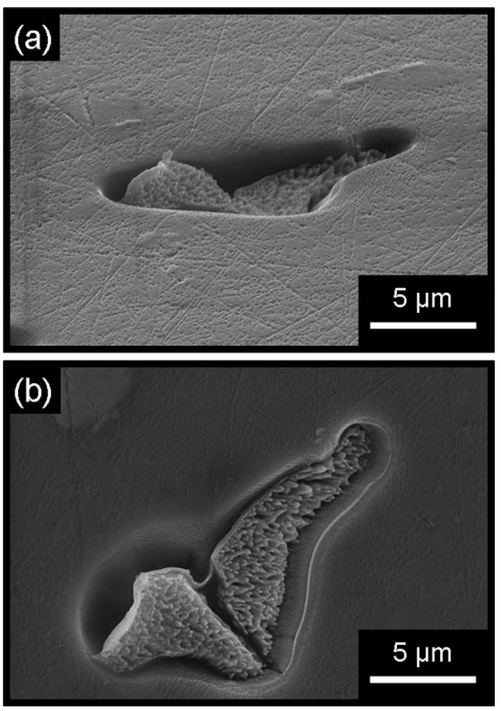

Figure 12. SEM observations of an S-phase particle in a (a) 70° tilted AA2024 specimen and (b) not tilted AA2024 specimen after immersion for 180 min in a 0.1 M Na_2SO_4 + 0.001 M NaCl solution at open-circuit potential.

the electron beam and the material, but it may suggest the formation of a Cu_2O oxide film, which is in good agreement with literature.[16]

In summary, this statistical study allows a quantitative dissolution mechanism to be proposed for the S-phase particles of AA2024;

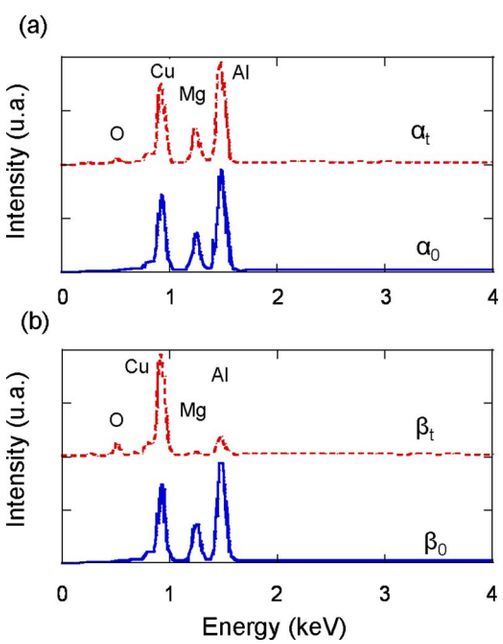

Figure 11. (Color online) EDS analyzes on the (a) α and (b) β zone marked out in Fig. 10 before (solid curve) and after (dotted curve) immersion for 30 min in a 0.1 M Na_2SO_4 + 0.001 M NaCl solution at open-circuit potential.

when an S-phase particle is attacked, its chemical composition changes (the copper content increases while the aluminum and magnesium contents decrease) until its copper content reaches about 60–70 atom %, corresponding to the formation of a probable Cu_2O-rich oxide film on the surface of the particle. This copper enrichment of the S-phase particle parallels a decrease of its potential relative to the matrix down to around −410 mV. Then, the SKPFM potential and the chemical composition of the particle do not evolve any longer while the dissolution depth continues to increase. Figure 12 shows that corroded S-phase particles have a porous structure arising from heterogeneous dissolution with preferential removal of aluminum and magnesium, leading to copper enrichment.[34,35] It can be assumed that, subsequent to the formation of the pores in the particle, settling of the structure occurs, which would explain the increase of the dissolution depth while neither the chemical composition nor the SKPFM potential continue to change. Furthermore, due to the copper enrichment, the particle becomes nobler. Oxygen reduction increases on the particle mainly at the particle/matrix interface favoring the dissolution of the surrounding matrix, as observed. When the dissolution of the matrix is so strong that there is no longer any mechanical cohesion with the particle, the particle falls out; the potential measured on this site is then that of the matrix (Fig. 5). As a conclusion, when an S-particle is corroded, particle dealloying is observed as well as the formation of a groove around the perimeter of the particle due to increased oxygen reduction on the particle and subsequent alkalinization at the interface particle/matrix.

Conclusion

AFM, SKPFM, and EDS experiments were performed on more than 300 Al_2CuMg particles in AA2024 to study their dissolution in chloride-containing solutions. The results show that (*i*) statistical analysis is necessary for quantitative measurements because the dissolution kinetics of the S-phase particles varies strongly from one intermetallic to another, (*ii*) dissolution of the S-phase particles oc-

curs with release of magnesium into the solution resulting in copper enrichment, (*iii*) dissolution kinetics of S-phase particles can be followed by SKPFM potential measurements because the copper enrichment of the particles parallels a decrease of their potential relative to the matrix. Due to the copper enrichment, the particles become nobler than the matrix and hence favor the dissolution of the surrounding matrix. The particles finally fall from the surface of the material and then there is no longer potential contrast; and (*iv*) even though the measurements are not so trivial to interpret, SKPFM potentials are found to be a powerful tool to follow the dissolution kinetics of intermetallics.

Centre National de la Recherche Scientifique assisted in meeting the publication costs of this article.

References

1. Z. Szklarska-Smialowska, *Corros. Sci.*, **41**, 1743 (1999).
2. J. W. J. Silva, A. G. Bustamante, E. N. Codaro, R. Z. Nakazato, and L. R. O. Hein, *Appl. Surf. Sci.*, **236**, 356 (2004).
3. A. Garner and D. Tromans, *Corrosion (Houston)*, **35**, 55 (1979).
4. X. Zhao, G. S. Frankel, B. Zoofan, and S. Rokhlin, *Corrosion (Houston)*, **59**, 1012 (2003).
5. M. Posada, L. E. Murr, C. S. Niou, D. Roberson, D. Little, R. Arrowood, and D. George, *Mater. Charact.*, **38**, 259 (1997).
6. M. R. Bayoumi, *Eng. Fract. Mech.*, **54**, 879 (1996).
7. X. Liu, G. S. Frankel, B. Zoofan, and S. Rokhlin, *Corros. Sci.*, **49**, 139 (2007).
8. I. L. Muller and J. R. Galvele, *Corros. Sci.*, **17**, 179 (1977).
9. J. F. Li, Z. Ziqiao, J. Na, and T. Chengyu, *Mater. Chem. Phys.*, **91**, 325 (2005).
10. J. Galvele and S. De Micheli, *Corros. Sci.*, **10**, 795 (1970).
11. V. Guillaumin and G. Mankowski, *Corros. Sci.*, **41**, 421 (1998).
12. W. Zhang and G. S. Frankel, *Electrochim. Acta*, **48**, 1193 (2003).
13. C. Blanc, B. Lavelle, and G. Mankowski, *Corros. Sci.*, **39**, 495 (1997).
14. R. G. Buchheit, L. P. Montes, M. A. Martinez, J. Michael, and P. F. Hlava, *J. Electrochem. Soc.*, **146**, 4424 (1999).
15. N. Birbilis and R. G. Buchheit, *J. Electrochem. Soc.*, **152**, B140 (2005).
16. C. Blanc, A. Freulon, M. C. Lafont, Y. Kihn, and G. Mankowski, *Corros. Sci.*, **48**, 3838 (2006).
17. C. Blanc, S. Gastaud, and G. Mankowski, *J. Electrochem. Soc.*, **150**, B396 (2003).
18. R. G. Buchheit, R. P. Grant, P. F. Hlava, B. Mckenzie, and G. L. Zender, *J. Electrochem. Soc.*, **144**, 2621 (1997).
19. Y. Yoon and R. G. Buchheit, *J. Electrochem. Soc.*, **153**, B151 (2006).
20. P. Schmutz and G. S. Frankel, *J. Electrochem. Soc.*, **145**, 2285 (1998).
21. P. Schmutz and G. S. Frankel, *J. Electrochem. Soc.*, **145**, 2295 (1998).
22. V. Guillaumin, P. Schmutz, and G. S. Frankel, *J. Electrochem. Soc.*, **148**, B163 (2001).
23. P. Leblanc and G. S. Frankel, *J. Electrochem. Soc.*, **149**, B239 (2002).
24. T. H. Muster and A. E. Hughes, *J. Electrochem. Soc.*, **153**, B474 (2006).
25. H. O. Jacobs, H. F. Knapp, S. Müller, and A. Stemmer, *Ultramicroscopy*, **69**, 39 (1997).
26. J. H. W. de Wit, *Electrochim. Acta*, **49**, 2841 (2004).
27. M. Rohwerder and F. Turcu, *Electrochim. Acta*, **53**, 290 (2007).
28. H. O. Jacobs, P. Leuchtmann, O. J. Homan, and A. Stemmer, *J. Appl. Phys.*, **84**, 1168 (1998).
29. T. Ouisse, F. Martins, M. Stark, and S. Huant, *Appl. Phys. Lett.*, **88**, 043102 (2006).
30. H. O. Jacobs, H. F. Knapp, and A. Stemmer, *Rev. Sci. Instrum.*, **70**, 1756 (1999).
31. B. S. Tanem, G. Svenningsen, and J. Mardalen, *Corros. Sci.*, **47**, 1506 (2005).
32. N. Gaillard, M. Gros-Jean, D. Mariolle, F. Bertin, and A. Bsiesy, *Appl. Phys. Lett.*, **89**, 154101 (2006).
33. J. Idrac, P. Skeldon, Y. Liu, T. Hashimoto, G. Mankowski, G. Thompson, and C. Blanc, in *Proceedings of the 9th International Symposium on the Passivation of Metals and Semiconductors and the Properties of Thin Oxide Layers*, P. Marcus and V. Maurice, Editors, pp. 167–172, Elsevier B.V., Amsterdam (2006).
34. T. Suter and R. C. Alkire, *J. Electrochem. Soc.*, **148**, B36 (2001).
35. R. G. Buchheit, M. A. Martinez, and L. P. Montes, *J. Electrochem. Soc.*, **147**, 119 (2000).